Compositional and Microstructural Changes Which Attend Reheating and Grain Coarsening in Steels Containing Niobium

E.J. PALMIERE, C.I. GARCIA, and A.J. DeARDO

This work describes the effect of temperature on both the microstructure and composition of microalloyed steel austenite in the as-reheated condition. Four laboratory steels of similar C levels were analyzed in this investigation. Three steels had different Nb concentrations at constant N levels, and the fourth exhibited a difference in N concentration. The average prior-austenite grain size was determined using quantitative metallographic techniques as a function of reheat temperature. The corresponding amount of Nb in solution in austenite was determined from atom probe analysis. Results from this investigation indicate that at elevated temperatures, representative of typical reheating practice, a smaller amount of Nb is soluble in austenite than what would have been predicted from any existing solubility relation for NbC_x in austenite. The solubility of Nb and C in austenite for the low-N steels is described by the relation: Log [Nb][C] $= 2.06 - 6700/T$. Additionally, it is shown that undissolved NbC_x particles are present in austenite approximately 125 °C above the grain-coarsening temperature.

I. INTRODUCTION

THE influence of microalloying elements such as Nb on the response of austenite to thermomechanical processing can be understood by the way in which Nb affects the three critical temperatures of austenite. These temperatures are the grain-coarsening temperature (T_{GC}), the recrystallization-stop temperature (T_{RXN}), and the transformation temperature (Ar_3 or B_s).[1-4] While all three of these temperatures are important to the effectiveness of thermomechanical processing, this present study focuses only on the T_{GC}. The T_{GC} is defined as that temperature above which abnormal grain coarsening or secondary recrystallization commences. This temperature can be considered where an equilibrium exists between the driving force for grain coarsening and the pinning force opposing boundary motion. The driving force is taken to be inversely related to the initial grain diameter, while the pinning force is related to the ratio of the particle volume fraction to the particle radius. The pinning force is, therefore, governed by the thermodynamic stability of second-phase particles in austenite.[5,6,7] Since the reheating of slabs or billets represents the initial stage for a given deformation process, knowledge of where the T_{GC} exists relative to the reheating temperature (T_{RHT}) is important. Hence, vastly different microstructures and microalloy solute levels can result depending upon whether the steel has been reheated above or below the T_{GC}.

The reheating practice is usually dictated by the requirements of the final product. For example, in products where toughness is very important (*e.g.*, high-strength plate), reheating can take place below the T_{GC} such that grain coarsening is kept to a minimum. In this case, second-phase particles remain relatively undissolved in austenite and will not be available for strengthening by reprecipitation during subsequent processing. Therefore, products such as high-strength plate are able to achieve the combined benefits of high-strength and low-impact transition temperatures through grain and subgrain refinement.[1] Conversely, for products where the toughness is not as important as strength (*e.g.*, strip), reheating can take place above the T_{GC}. Hence, although some coarsening may occur during strip processing when $T_{RHT} > T_{GC}$, most of the microalloying elements are put into solution in austenite. These elements in solution are thus available for precipitation strengthening during deformation and/or after the ferrite or bainite transformation.[8-11] However, the ability to choose a particular reheat practice can only be accomplished through an understanding of the T_{GC} and those elements which affect it. The present investigation has considered the solution behavior of Nb, C, and N in austenite and their effect on the T_{GC} of the austenite.

A. *Solubility of Nb Carbonitrides in Austenite*

The crystal structure of γ-NbC_x can be represented by two interpenetrating fcc lattices with Nb atoms or Nb atom vacancies occupying one set of lattice sites and C atoms or C atom vacancies occupying the other set of lattice sites.[12] The compound δ-NbN_y would likewise exhibit the same crystal structure.[13] The compounds NbC_x and NbN_y have complete solid solubility which enable them to form a carbonitride, NbC_xN_y, where x equals the atomic ratio C/Nb, y equals the atomic ratio N/Nb and $1 - (x + y)$ equals the atomic ratio of vacancies.[12] Storms and Krikorian[14] have reported that the lattice parameter of NbC_xN_y (henceforth referred to as Nb(CN)) varies with both vacancy concentration and C/N ratio. More recent work by Balasubramanian *et al.*[15] using a two-sublattice model has also shown the variation in NbC_x solubility in austenite as a function of lattice-site occupancy. The solubility of NbC_x in austenite increases as fewer C atoms occupy positions in the

E.J. PALMIERE, Assistant Professor, C.I. GARCIA, Associate Research Professor, and A.J. DeARDO, Professor, are with the Department of Materials Science and Engineering, University of Pittsburgh, Pittsburgh, PA 15261.

Manuscript submitted February 17, 1993.

second interstitial sublattice sites. Hence, as x in NbC_x decreases from unity, the solubility of the compound in austenite increases.

The importance of Nb as a microalloying element in steels is apparent from the numerous studies performed over the past 30 years. Much of this work was concentrated on the solubility of Nb monocarbides,[12,15-27] mononitrides,[12,15,16,22,24,28,29] and carbonitrides[12,15,30-34] in austenite. The results of these studies are shown in Table I in the form of solubility products. The differences among these products are considerable and may be attributed to a number of reasons. Foremost among these reasons is the variety of methods used in obtaining the given solubility, as each technique has its own assumptions and limitations. The techniques used in obtaining the solubility products of Table I are classified as A through E and are briefly described in the following:

(A) thermodynamic calculations;
(B) chemical separation and isolation of precipitate;
(C) equilibrating a series of steels with different Nb concentrations in a H_2-CH_4 atmosphere at various temperatures, after which the C contents are analyzed;
(D) hardness measurements; and
(E) statistical treatment of existing solubility products.

Thermodynamic calculations of solubility products often neglect any interaction between elements. As a result, the activity coefficients are assumed to be unity and the activities are represented by their weight percents. Recent work, however, has incorporated Wagner interaction parameters to account for the effect of alloying elements on the solubility of Nb(CN) in austenite.[15,24] This leads to a more realistic solubility product since it incorporates nonunity activity coefficients.

Although techniques such as chemical separation and methane equilibration indirectly account for chemical interactions, both have their own limitations. One problem arising from the separation technique is that very fine precipitates may not be included in the analysis and that discrepancies may exist as to the exact composition of the precipitate.[16,25] This problem also occurs in the equilibration methods, as carbon contents are often analyzed assuming that a stoichiometric or nonstoichiometric compound is present.[25] Additionally, both of these methods, including the thermodynamic calculations, neglect the effect of precipitate size on solubility. Thermodynamics indicate that small particles are more soluble than large particles.[35] Hence, solubility products obtained from these techniques may predict a more stable precipitate than would be expected.

Finally, hardness techniques are questionable since they are based upon the assumption that an increase in hardness is proportional to the amount of Nb dissolved in austenite and subsequently precipitated in ferrite as Nb(CN).[16] Although this does indeed occur, all of the C and N present in the steel is not necessarily associated with the precipitate. Also, difficulties arise in separating this hardness increment from those due to other mechanisms such as grain size, solid solution, and dislocation strengthening.

In summary, all of the solubility products represented in Table I are useful in providing a general understanding of Nb(CN) solubility in austenite. The goal of this research is to provide a more detailed understanding of

Table I. Solubility Products for Nb-C, Nb-N, and Nb-C-N Systems in Austenite

System	Product	Method	Reference
Nb-C	$\log [Nb][C] = 2.9 - 7500/T$	D	17
	$\log [Nb][C] = 3.04 - 7290/T$	B	18
	$\log [Nb][C] = 3.7 - 9100/T$	C	19
	$\log [Nb][C] = 3.42 - 7900/T$	B	20
	$\log [Nb][C] = 4.37 - 9290/T$	C	21
	$\log [Nb][C]^{0.87} = 3.18 - 7700/T$	B	22
	$\log [Nb][C]^{0.87} = 3.11 - 7520/T$	E	16
	$\log [Nb][C] = 2.96 - 7510/T$	E	16
	$\log [Nb][C]^{0.87} = 3.4 - 7200/T$	A	16
	$\log [Nb][C] = 3.31 - 7970/T +$ $[Mn](1371/T - 0.9) - [Mn]^2(75/T - 0.0504)$	B	23
	$\log [Nb][C]^{0.87} = 2.81 - 7019.5/T$	A	24
	$\log [Nb][C]^{0.87} = 3.4 - 7920/T$	C	25
	$\log [Nb][C] = 1.18 - 4880/T$	C	26
	$\log [Nb][C] = 1.74 - 5600/T$	C	27
	$\log [Nb][C] = 3.89 - 8030/T$	C	15
Nb-N	$\log [Nb][N] = 4.04 - 10{,}230/T$	C	29
	$\log [Nb][N] = 3.79 - 10{,}150/T$	B	22
	$\log [Nb][N] = 2.8 - 8500/T$	B	20
	$\log [Nb][N] = 3.7 - 10{,}800/T$	B	31
	$\log [Nb][N]^{0.87} = 2.86 - 7927/T$	A	24
	$\log [Nb][N] = 4.2 - 10{,}000/T$		28
Nb-C-N	$\log [Nb][C]^{0.24}[N]^{0.85} = 4.09 - 10{,}500/T$	B	16
	$\log [Nb][C + 12/14N] = 3.97 - 8800/T$	C	32
	$\log [Nb][C + N] = 1.54 - 5860/T$	B	16
	$\log [Nb][C]^{0.83}[N]^{0.14} = 4.46 - 9800/T$	B	16
	$\log [Nb][C + 12/14N] = 2.26 - 6770/T$	C	30

this behavior and the effects of this behavior on austenite grain coarsening during reheating.

II. EXPERIMENTAL PROCEDURE

This investigation involved the use of a series of low-C, Si-killed laboratory steels having compositions shown in Table II. The choice of Si as a deoxidizer as opposed to Al was made to minimize any effects of Aluminum-nitride (AlN) precipitation, which could complicate the analysis. For all steels, the soluble O levels were no greater than 6 ppm. Further analysis revealed that the total amount of residual elements detected did not exceed 0.016 at. pct. A relatively high concentration of Mn was used in order to provide added hardenability to minimize the amount of proeutectoid ferrite formation during quenching.[36,37,38] This was required so that an accurate description of the prior-austenite grain size could be attained. The amount of S in these steels was chosen to represent standard levels in grades where machinability of the final product is not a critical factor.[39] The P level was intentionally kept high to assist in metallographic techniques associated with revealing prior-austenite grain boundaries.[32,40]

A. *Material Processing*

The base steel (E0) had a C and N concentration of 0.415 and 0.032 at. pct (0.09 and 0.008 wt pct), respectively. Four grades of steel (E1 to E4) microalloyed with Nb were subsequently formulated around this base steel. Three of these steels (E1, E3, and E4) had similar N levels with varying Nb concentrations. Two steels (E1 and E2) contained the same Nb concentrations with different N levels. Hence, regardless of which solubility relation employed from the literature, as represented by Table I, these steels should display three different forms of Nb solution behavior in austenite.

All laboratory steels were vacuum induction-melted and received in their as-cast condition in the form of 11.4 to 22.7 kg ingots. This material subsequently experienced a homogenization treatment and was rolled into bars approximately 16 mm in diameter. These bars were further machined into right cylinders having a height and diameter of 12.7 mm for reheating studies.

Table II. Steel Compositions

	Composition in Atomic Percent (Weight Percent)				
Element	E0	E1	E2	E3	E4
C	0.415	0.415	0.369	0.369	0.370
	(0.090)	(0.090)	(0.080)	(0.080)	(0.080)
Mn	1.503	1.503	1.483	1.453	1.445
	(1.490)	(1.490)	(1.470)	(1.440)	(1.430)
P	0.016	0.016	0.016	0.014	0.018
	(0.009)	(0.009)	(0.009)	(0.008)	(0.010)
S	0.010	0.021	0.010	0.010	0.010
	(0.006)	(0.012)	(0.006)	(0.006)	(0.006)
Si	0.809	0.809	0.809	0.789	0.573
	(0.410)	(0.410)	(0.410)	(0.400)	(0.290)
Nb		0.029	0.029	0.012	0.054
		(0.049)	(0.048)	(0.020)	(0.090)
N	0.032	0.032	0.095	0.032	0.032
	(0.008)	(0.008)	(0.024)	(0.008)	(0.008)

B. *Grain-Coarsening Studies*

In order to ascertain both the prior-austenite grain size and the amount of soluble Nb as a function of temperature, isothermal reheating studies were performed on the steel specimens. Prior to each austenitizing treatment, specimens were placed in evacuated quartz tubes backfilled with dry argon (99.9 pct purity). Therefore, the total pressure of each sealed tube was measured at 100 mtorr.

Eight different temperatures spanning the austenite phase field were employed for the reheating studies. The highest test temperature was 1300 °C, whereas the lowest temperature was 950 °C. The remaining six temperatures were at 50 °C increments within this range. The reason for selecting 1300 °C as the upper reheating temperature is shown in Table III. Table III shows the average temperatures above which complete solubility in austenite occurs for a Nb monocarbide, mononitride, and carbonitride. The temperatures represented by Table III were calculated from the solubility products shown in Table I. Based on the values shown in Table III, reheating at 1300 °C would be expected to ensure the complete dissolution of precipitates for all steels. For the least thermodynamically stable precipitate (*i.e.*, greatest solubility in austenite), reheating would be expected to occur 290 °C above the precipitate dissolution temperature. Alternatively, reheating at 1300 °C would occur 46 °C above the precipitate dissolution temperature for the most thermodynamically stable precipitate (*i.e.*, smallest solubility in austenite).

Following equilibration of the furnace at the respective reheat temperatures, specimens were austenitized for 30 minutes at that temperature. The heating rate of the specimens was approximately 5 °C/sec. Immediately following reheating, specimens were water-quenched in an iced water bath. Specimens were then sectioned in two halves. The first half was tempered at 500 °C in an Ar atmosphere for 24 hours. This treatment was performed to aid in optical metallographic techniques by allowing phosphorus in solution to segregate toward the austenite grain boundaries.[32] The second half of the cylindrical specimen was held in the as-quenched condition for later analysis using atom probe analysis and field ion microscopy.

Table III. Average Precipitate Dissolution Temperature as Calculated from Table I

	Average Precipitate Dissolution Temperature in °C (Calculated from Table I)		
Steel	Nb-C	Nb-N	Nb-C-N
E1	1114 (59)	1112 (75)	1188 (53)
E2	1099 (58)	1254 (94)	1203 (69)
E3	1010 (56)	1038 (73)	1081 (41)
E4	1172 (63)	1167 (77)	1251 (68)

Values in parentheses represent standard deviations.

All field ion microscopy was performed between 40 and 50 K using Ne as an imaging gas. Imaging was performed at $2.5 \cdot 10^{-5}$ torr neon. Atom probe analysis was conducted at 60 K. This temperature was selected to minimize the field-induced stresses imposed on the specimens, permitting a longer tip life during which ions could be collected. Analysis was performed in the presence of 10^{-8} to $5 \cdot 10^{-9}$ torr neon.

III. RESULTS AND DISCUSSION

A. *Microstructure of Austenite*

The prior-austenite grain size as a function of reheating temperature for steel E1 is shown in Figure 1. This sequence of microstructures appears to be fully martensitic with no evidence of proeutectoid ferrite formation along prior-austenite grain boundaries. All other steels displayed similar microstructures. The overall coarsening behavior with reheating temperature is illustrated for all of the steels in Figure 2. The grain-coarsening behavior of the plain C steel (E0) is indicative of normal grain coarsening in that the grain size systematically increases with increasing temperature while maintaining a consistent normal distribution. The three microalloyed steels, however, exhibited abnormal grain coarsening which is often referred to as secondary recrystallization.[5,41]

Abnormal grain coarsening occurs when the newly formed austenite grains are kept fine by the presence of a distribution of second-phase particles such as Nb(CN). Gladman[5,42] showed that there exists a critical condition where the energy release rate per unit displacement of grain boundary during grain coarsening is equal to the rate of energy release due to the absence of particle pinning. He defined this condition in terms of a critical particle radius, r_{crit}, which represents the maximum particle size that would effectively counteract the driving force for austenite grain coarsening.

$$r_{crit} = \frac{6R_0 f}{\pi}\left(\frac{3}{2} - \frac{2}{Z}\right)^{-1} \quad [1]$$

In this expression, R_0 is the initial matrix grain size, f is the volume fraction of particles, and Z is a term used to account for the heterogeneity of the matrix grain size. It is clear from Eq. [1] that for some given uniform initial grain size, r_{crit} will be the product of some constant and the particulate volume fraction. Hence, it will be the volume fraction of precipitate which will influence r_{crit}. This volume fraction will be sensitive to temperature as defined by the solubility relationship of the precipitating compound. Therefore, as the temperature increases, progressively increasing amounts of Nb, C, and N go into solution in austenite.[42,43] The result of this is that the volume fraction of Nb(CN) particles available to retard grain coarsening decreases. This situation leads to the coarsening of some grains at the expense of others, while some remaining grains continue to be pinned. Hence, a bimodal grain-size distribution develops that is clearly distinguished from the single grain-size distribution associated with normal grain coarsening.

The grain-coarsening characteristics of the experimental steels are shown in Figure 2. Three regimes of behavior can be defined for the microalloyed steels. With increasing temperature, these regimes represent: (1) a unimodal distribution of the initial grains exhibiting suppressed normal grain coarsening, (2) a bimodal distribution of retained primary and new abnormally coarsened grains, and (3) a unimodal distribution of abnormally coarsened grains exhibiting accelerated normal grain coarsening. Based on the curves of Figure 2, the beginning of abnormal grain coarsening and, hence, the T_{GC} can be defined by the onset of the second regime.[7] In Figure 2, this is represented by the temperature where there is a discontinuity in the average austenite grain diameter. The discontinuity arises because two clearly distinguishable average austenite grain diameters have been measured. Depending on the chemical composition of the steel, this bimodal grain distribution exhibited in regime 2 can occur over various temperatures. The highest T_{GC} would, therefore, be expected for the most thermodynamically stable precipitate, *i.e.*, the precipitate associated with the smallest solubility product. Hence, as illustrated in Figure 2, the respective T_{GC} in ascending order for steels E3, E1, E2, and E4 are 1000 °C, 1100 °C, 1150 °C, and 1200 °C.

The trend of increasing T_{GC} with nominal N or Nb

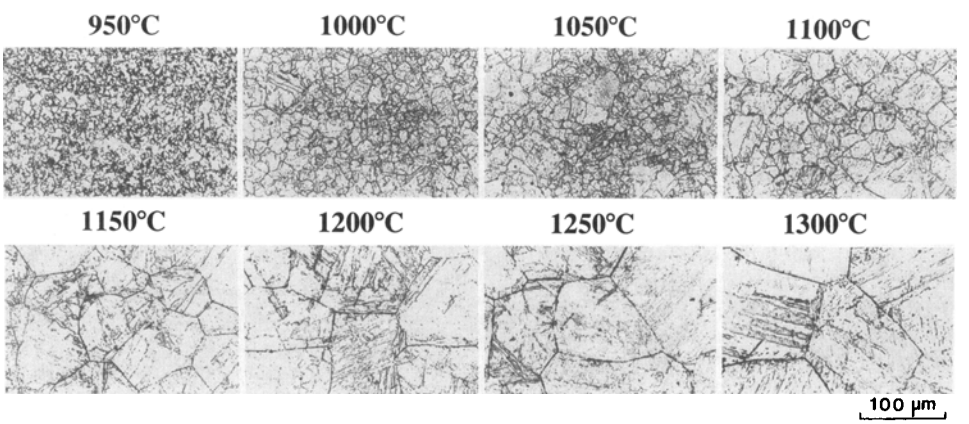

Fig. 1 — Prior-austenite grain size for steel E1 after isothermally reheating to the above temperatures and water quenching. This steel had a grain-coarsening temperature of 1100 °C.

levels is in agreement with observations from previous studies.[3,5,8,11,30,32,44] The implication of this, as stated previously, is that a high T_{GC} will result in those systems in which precipitates are most stable. Since the C level was essentially similar for all of the steels, the T_{GC} was found to increase systematically with Nb concentration for steels E3, E1, and E4. These three steels had similar N concentrations. Alternatively, the T_{GC} was found to increase with increasing N levels at constant C and Nb concentrations. This behavior is observed by comparing the curves for steels E1 and E2 in Figure 2. These results indicate that, as initially hypothesized, austenite grain coarsening is most effectively retarded by high-stability precipitates, since they are the least soluble in austenite. This translates into a higher volume fraction of fine Nb(CN) precipitates available to retard grain coarsening at elevated temperatures.

As the reheating temperature further increases above the T_{GC} into regime three behavior, the curves presented in Figure 2 reassume an appearance indicative of normal grain coarsening.[32] This form of grain coarsening in the microalloyed steels results because at these temperatures, nearly all of the precipitate is dissolved in austenite. Hence, only a small volume fraction of precipitate remains to retard grain coarsening. These remaining particles, however, are ineffective because they are coarse.[5] Additionally, the interparticle spacing between these precipitates is large. The combined effects of having a relatively small number of coarse particles with large interparticle spacings render the coarsening of austenite grains for steels E1 through E4 similar to the coarsening of single-phase austenite.

B. *Composition of Austenite*

Atom probe analysis was used to determine the amount of Nb soluble in austenite as a function of reheating temperature. This technique consisted of the bulk random analysis of at least 100,000 ions per steel and condition. These ions were collected from an average of 10 to 15 specimens, each taken from a different location in the bulk steel. The results are shown in Figure 3 for steels E1 to E4. Before interpreting the results of Figure 3, a few comments are necessary regarding the data contained within this figure. First, each data point represents an absolute Nb concentration rather than a relative concentration. For example, out of the 106,014 ions collected for steel E1 reheated at 1100 °C, 32 ions were Nb. This translates into a Nb concentration of 0.030 at. pct, which agrees with the bulk chemistry analysis shown in Table II. Of the 32 total Nb ions, 18 ions were not associated with either C or N ions (*i.e.*, the separation between Nb and either C or N ions was at least four atomic planes). Hence, for this steel and condition, 0.017 at. pct Nb was in solution in austenite, while the remaining Nb was associated with C in the form of NbC_x. It should be noted that Nb(CN) particles were not observed in any of the low-N steels. The final point to be made regarding the data represented in Figure 3 concerns the statistical scatter. Indeed, this was a very important consideration and was the primary reason for the analysis of a large number of ions for each steel and condition. Assuming a normal distribution, the

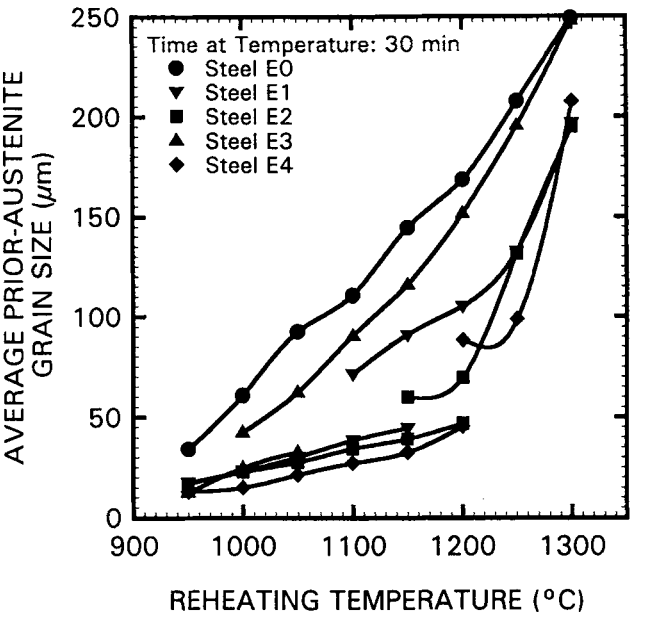

Fig. 2—Prior-austenite grain size as a function of reheating temperature for both the plain-carbon steel and the steels microalloyed with Nb.

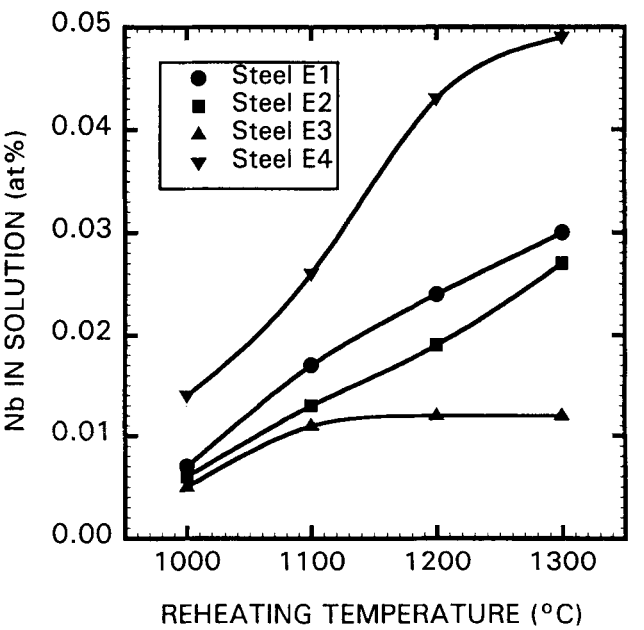

Fig. 3—Nb in solution in austenite as a function of reheating temperature determined from atom probe analysis.

standard error about each data point in Figure 3 was found to be no greater than 0.005 at. pct.

Field ion microscopy revealed that the precipitates in all of the microalloyed steels ranged in size from 0.5 to 10 nm. Furthermore, atom probe analysis showed that the low-N containing steels had particle compositions ranging from $NbC_{0.8}$ to stoichiometric NbC. An example of a very fine NbC precipitate is shown in Figure 4 with a corresponding chemical analysis shown in Figure 5. Figures 4 and 5 indicate that this precipitate is on the order of 1 nm and has a stoichiometric composition NbC. The reason that Figure 5 does not indicate a more

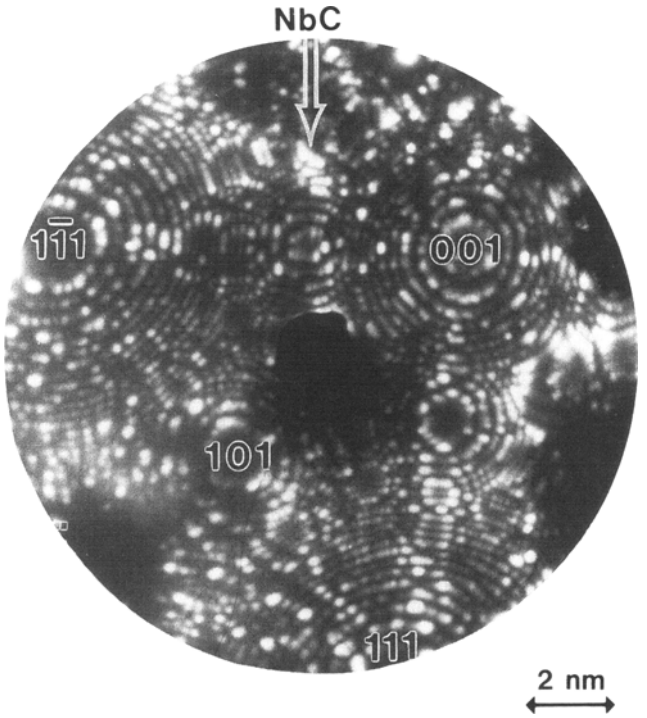

Fig. 4—Field ion micrograph depicting an NbC precipitate in steel E1, reheated to 1000 °C and water-quenched.

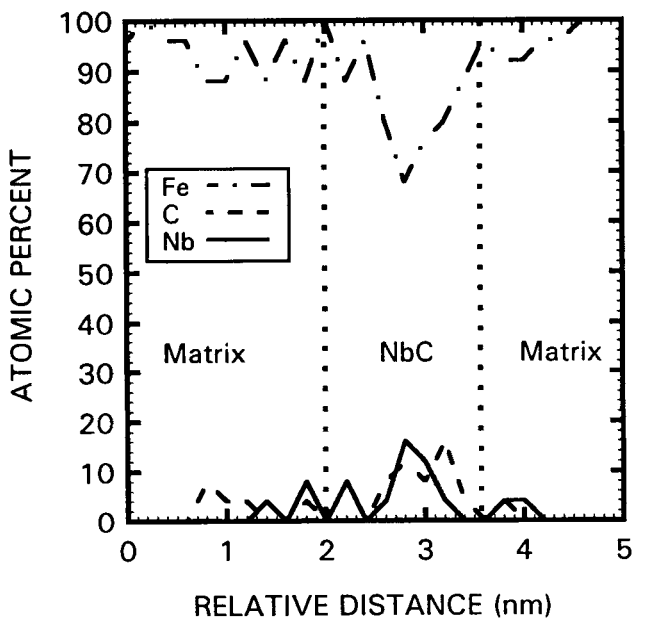

Fig. 5—Atom probe analysis of NbC precipitate in steel E1, reheated to 1000 °C and water-quenched.

dramatic decrease in Fe and increase in both Nb and C is attributed to the size of the precipitate. Since the size of the precipitate is smaller than the probe aperture (≈3 nm), a portion of the matrix is included in the analysis along with the precipitate.

It was also possible, albeit with a smaller degree of certainty, to elucidate the compositional ranges for the N-rich precipitates found in steel E2. These precipitates ranged in composition from $NbC_{0.67}N_{0.33}$ to $NbC_{0.8}N_{0.07}$. The uncertainty in these compositions is due to the fact that both the N and Si field evaporate with similar mass-to-charge (m/n) ratios (N^{+1}, Si^{+2} ∴ m/n = 14). It should be mentioned, however, that unlike pure Nb carbides, the presence of either pure Nb nitrides or Nb silicides was not detected. Hence, other than being detected in an uncombined form with other elements, N (and Si) were always found in association with Nb and C. It was this observation which led to the deduction that the precipitate was of the form Nb(CN).

The curves in Figure 3 offer further support for the grain-coarsening results shown in Figure 2. If the two steels (E1 and E2) of similar Nb levels are compared, it is observed that at any reheating temperature, the steel with the high-N concentration shows less Nb in solution in austenite. This points to the stabilizing effect associated with increased N contents in Nb(CN). Since there are no other elements present in these steels which have a higher affinity for N than Nb, a N-rich Nb(CN) precipitate would be expected. The increased stability of this N-rich precipitate in austenite would lead to a smaller solubility of Nb in austenite at any reheating temperature. This is particularly evident at the reheat temperature of 1300 °C where essentially all of the Nb contained in steel E1 is in solution, whereas only ~93 pct of the Nb contained in steel E2 is in solution in austenite. The result is that a larger volume fraction of particles are able to retard grain coarsening and explains the higher T_{GC} for steel E2 relative to steel E1. Additionally, as these particles exhibit a lower solubility in austenite, they do not experience significant coarsening.[35] Therefore, it is through the combined effect of a large volume fraction of small undissolved Nb(CN) particles which enables the T_{GC} of steel E2 to be 50 °C higher than that of steel E1.

The interesting point to be made from Figures 2 and 3 is that complete solubility of Nb in austenite is not observed at reheating temperatures as high as 200 °C above the respective T_{GC} for each steel. This is in contrast to other investigations[45,46,47] which reported that Nb(CN) precipitates were completely dissolved in austenite at temperatures 70 °C to 100 °C higher than the T_{GC}. The reason for this inconsistency is that the previous studies calculated the solution behavior of Nb in austenite using one or more of the solubility expressions given in Table I. Hence, the solubility products listed in Table I result in an overestimation of the amount of Nb in solution in austenite. This overestimation can be observed when the solubility products represented in Table I are plotted over the temperature range 1000 °C through 1300 °C (Figure 6). Incorporated into Figure 6 is a solubility relationship from the present study. This relationship was determined using the measured atom probe results from steel E3 for the solution behavior of Nb in austenite. The amount of C in solution was calculated from these data assuming a stoichiometric precipitate NbC. Using this technique, the following solubility product was obtained:

$$\text{Log [Nb][C]} = 2.06 - \frac{6700}{T} \qquad [2]$$

In conformity with those products listed in Table I,

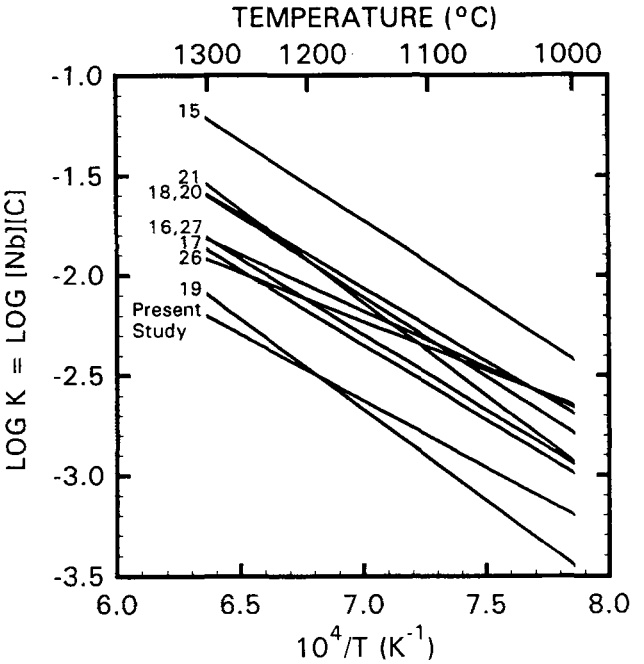

Fig. 6—Solubility products for stoichiometric NbC in austenite as a function of temperature. The numbers to the left of each curve correspond to those products listed in Table I.

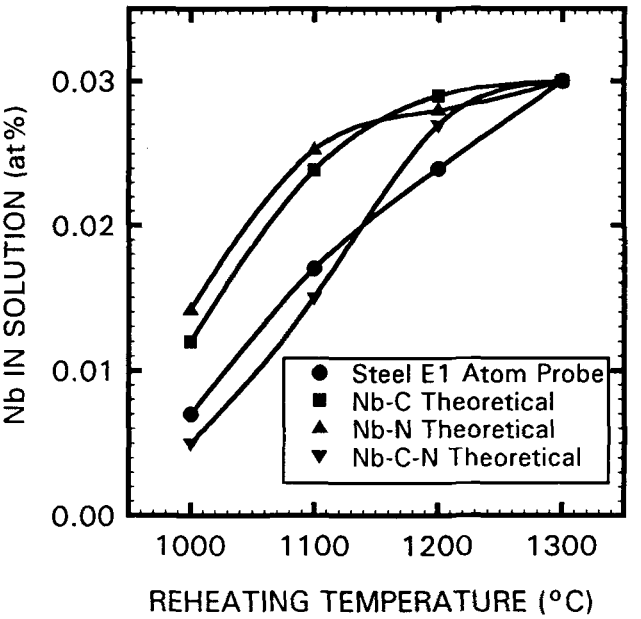

Fig. 7—Nb in solution in austenite *vs* reheating temperature. A comparison is presented between the results of steel E1 obtained by atom probe analysis and what would be predicted from the solubility products listed in Table I. Each of the theoretical values were calculated form solubility products that were averaged from that type of precipitate.

the concentrations of [Nb] and [C] are given by their wt pct. This solubility product would predict a dissolution temperature of 1107 °C for steel E3, which is in very good agreement with the atom probe measurements illustrated in Figure 3. The magnitudes of both the entropic (2.06) and enthalpic ($-6700/T$) terms shown in Eq. [2] are comparable to those of the solubility products in Table I. The curve for the present study in Figure 6 displays two interesting features. First, the curve for steel E3 exhibits a weaker temperature dependence than most other curves, apparently due to the relatively small enthalpic contribution. Second, with the exception of the product of Smith,[19] the present product for steel E3 predicts a much lower solubility (*i.e.*, more stable precipitate) than any of the other products. This can be attributed to both enthalpic and entropic contributions.

Figure 7 shows a comparison of the amount of soluble Nb in austenite as determined from atom probe analysis and the amount of soluble Nb in austenite calculated from the solubility products listed in Table I. Each solubility product from Table I was categorized into one of the three different precipitating systems: Nb-C, Nb-N, and Nb-C-N. The average value calculated from the solubility products within each system is represented in Figure 7.

It is apparent from Figure 7 that both the theoretical Nb-C or Nb-N curves indicate substantially higher levels of Nb in solution than the measured atom probe data of steel E1, which exhibits a nearly nitrogen-free precipitate. Most important, however, is the comparison between curves Nb-C-N and steel E1. In general, both of these curves are in close agreement over the temperature range 1000 °C to 1300 °C, taking into account the standard error of 0.005 at pct about each data point for steel E1. This further illustrates that the existing solubility products, even those for a carbonitride, overestimate the dissolution behavior of Nb in austenite. Upon closer inspection of these two curves, it appears that at temperatures less than 1130 °C, the data from atom probe analysis indicate a less thermodynamically stable precipitate than would be predicted from existing solubility relationships. At temperatures greater than 1130 °C, the opposite behavior is observed. The discrepancy between these two curves is attributed to the assumptions incorporated with the theoretical solubility expressions. As stated previously, two important assumptions made in the determination of theoretical solubility products were the neglect of particle size and solute interactions on the solubility of Nb in austenite. The failure to incorporate these two effects, however, can be significant. For example, Cahn[35,48,49] has shown that particles ≤5 nm can have a marked influence on precipitate solubility. Many particles encountered during atom probe analysis were found to be smaller than 5 nm, perhaps explaining the higher experimentally observed solubility of Nb in austenite compared to the theoretical Nb-C-N curve at temperatures less than 1130 °C. A particle size argument alone, however, does not explain the deviation at higher temperatures.

An Fe-C-Nb ternary (0.46 at. pct C to 0.03 at. pct Nb), with Nb and C levels similar to steel E1, was analyzed using the atom probe in an attempt to elucidate the effects of particle size and solute interaction on the solubility of Nb in austenite. The rationale behind this experiment was to compare atom probe data for steel E1 with those of the ternary alloy as a function of reheating temperature. If the curves were found to be similar, the influence of solute interactions deriving from the presence of Mn and Si could be ignored. On the other hand, if steel E1 and the ternary alloy exhibited different solution behavior of Nb, these differences could be explained by solute interactions. Field ion microscopy

performed on steel E1 and the ternary confirmed that they had precipitates of similar diameters. These diameters ranged between 0.5 to 10 nm. At temperatures greater than 1100 °C, the ternary alloy exhibited a less thermodynamically stable precipitate relative to that of steel E1. This behavior may suggest the importance of solute interactions on the solubility of Nb in austenite in steel E1.

Chipman[50] has investigated the effect of alloying elements on the activity coefficients of N and C in molten iron alloys. Those elements (Al, As, Co, Cu, Ni, P, S, Sb, Si, and Sn) which raise the activity coefficient of either N or C decrease their solubility in liquid iron. Conversely, those elements (Cr, Mn, Mo, Nb, Ta, Ti, V, and W) which lower the activity coefficient of either N or C increase their solubility in liquid iron. Regarding solute interactions in austenite, Koyama *et al.*[23] showed that the addition of Mn leads to an increase in the activity coefficient of Nb in austenite. However, he also found that the decrease in the activity coefficient of C was greater in magnitude. Hence, the addition of Mn was observed to increase the solubility of NbC in austenite. The effect of Mn on Nb solubility in austenite, however, could be countered by the presence of Si, a graphite and ferrite stabilizer. The presence of Si leads to an increase in the activity coefficient of C in austenite. Therefore, the net effect of both Mn and Si could act to decrease the solubility of Nb in austenite. This rationale is consistent with the atom probe analysis of the ternary alloy and steel E1.

The solubility of particles in austenite and its influence on the grain-coarsening behavior during reheating are summarized in Table IV. The first important feature shown in Table IV concerns the difference between the observed and calculated[16,20,30] particle dissolution temperatures for the various steels. The first step in calculating a dissolution temperature involves choosing the appropriate solubility product. This can only be accomplished once the particle composition is known for a particular steel. Hence, it is not correct to use a solubility product for Nb(CN) to describe the dissolution of NbC. In the present study, NbC_x was the primary particle found in the low-N steels. This is in contrast to the Nb(CN) found in the higher N steel (E2). For the case of the dissolution of NbC_x in austenite, it is interesting to compare the experimentally determined dissolution temperatures with those calculated from solubility products (Table IV). Three of these solubility products were taken from the literature.[16,20,30] The fourth was the new solubility product experimentally determined from atom probe results (Eq. [2]). The discrepancy between the experimental and calculated dissolution temperatures varied with the Nb content of the steel for the three products taken from the literature. This discrepancy increases with increasing bulk Nb levels. In contrast, the solubility product from the present study leads to dissolution temperatures that are much closer to those observed at all Nb levels.

Table IV also reveals information concerning the relationship between the grain-coarsening temperature and particle dissolution temperature. In an earlier study, the grain-coarsening temperature was found to be about 70 °C to 100 °C less than the dissolution temperature.[46] However, this earlier work used one of the previously reported solubility products[30] in calculating the dissolution temperature, which underestimates the observed dissolution temperature by approximately 40 °C to 100 °C (Table IV). In contrast, the calculated dissolution temperature in the present study, using Eq. [2], is 107 °C to 150 °C greater than the observed grain-coarsening temperature, while the experimentally determined dissolution temperature is 100 °C to 200 °C greater. Hence, grain-coarsening temperatures based on dissolution temperatures calculated from Eq. [2] should be much closer to experimental values and can be approximated by the following expression:

$$T_{GC} = T_{DISS} - 125\ °C \qquad [3]$$

where T_{DISS} is the dissolution temperature calculated using Eq. [2]. Accurate information concerning T_{GC} and T_{DISS} is important in the design of effective reheating practices since reheating below the T_{GC} promotes fine and uniform hot-rolled austenite grain structures, while reheating above the T_{DISS} promotes maximum potential for precipitation in either austenite or ferrite during subsequent processing.[51,52]

IV. CONCLUSIONS

The following conclusions can be made regarding the compositional and microstructural changes which attend reheating and grain coarsening in steels containing Nb.

Table IV. Summary of Grain-Coarsening Temperature, Precipitate Composition, and Dissolution Temperature

	Present Study							Conventional Calculations of T_{DISS} (°C)		
	Bulk Compositions (Wt Pct)			Precipitate	T_{DISS}^{OBS}	T_{DISS}^{CALC}	T_{GC}			
Steel	Nb	C	N	Composition	(°C)	(°C)	(°C)	Ref. 16	Ref. 20	Ref. 30
E1	0.049	0.090	0.008	$NbC_{0.8}$ NbC	~1300	1247	1100	1142	1096	1197*
E2	0.048	0.080	0.024	$NbC_{0.67}N_{0.33}$ $NbC_{0.8}N_{0.07}$	>1300	—	1150	—	—	1212
E3	0.020	0.080	0.008	$NbC_{0.8}$ NbC	1100	1107	1000	1032	998	1066*
E4	0.090	0.080	0.008	$NbC_{0.8}$ NbC	>1300	1321	1200	1199	1147	1264*

*Indicates that N concentration was not included in the calculation.

1. Upon reheating, abnormal grain coarsening was observed for all microalloyed steels. The grain-coarsening temperature was found to increase with increasing precipitate stability. The most thermodynamically stable precipitates resulted in a high T_{GC}. In ascending order, grain-coarsening temperatures of 1000 °C, 1100 °C, 1150 °C, and 1200 °C were observed for steels E3, E1, E2, and E4, respectively.
2. Microchemical analysis using the atom probe appeared to be a very powerful tool for determining the amount of Nb in solution in austenite during reheating. In general, the results from the atom probe analysis showed some disagreement with solubility products from the literature. This disagreement was observed in both the enthalpic and entropic contributions to the solubility product, and was manifested in markedly lower experimental solubility levels for Nb in austenite. Therefore, it appears that the measured data from the atom probe yielded a more reliable description of the solution behavior of Nb in austenite than did the techniques previously employed during other investigations.
3. The overestimation of soluble Nb in austenite may be attributed to the interaction between solute elements such as Mn and Si. These solute interactions affect the solubility of Nb in austenite through their influence on the activity coefficients of C and Nb.
4. Atom probe analysis indicated that precipitates ranged in size from 0.5 to 10 nm and had compositions ranging from $NbC_{0.8}$ to stoichiometric NbC. These precipitate compositions were found in the low-N steels. Nitrogen-rich precipitates ranged in composition from $NbC_{0.67}N_{0.33}$ to $NbC_{0.8}N_{0.07}$ and were observed in the high-N steel (E2).
5. With the exception of steels E1 and E3, a complete dissolution of NbC_x was not observed for any steel at reheating temperatures as high as 1300 °C. A solubility product was calculated based on the atom probe data measured for steel E3 and can be written, by assuming a stoichiometric NbC precipitate, as $\text{Log}\,[\text{Nb}][\text{C}] = 2.06 - 6700/T$.
6. Grain-coarsening temperatures based on dissolution temperatures calculated using the solubility product from the present investigation should be much closer to experimental values and can be approximated by $T_{GC} = T_{\text{DISS}} - 125$ °C.

ACKNOWLEDGMENTS

The authors would like to thank the David Taylor Research Laboratories of the United States Navy and the Niobium Products Company, Inc., for financial support of this research program. Additionally, the authors would like to thank Dr. S.S. Brenner for his valuable comments as well as for the use of the atom probe laboratory.

REFERENCES

1. F.B. Pickering: in *Microalloying 75*, M. Korchynsky, ed., Union Carbide Corporation, New York, NY, 1977, p. 9.
2. W.J. McG. Tegart and A. Gittins: in *The Hot Deformation of Austenite*, J.B. Ballance, ed., TMS-AIME, Warrendale, PA, 1977, p. 1.
3. P.K. Amin and F.B. Pickering: in *Thermomechanical Processing of Microalloyed Austenite*, A.J. DeArdo, G.A. Ratz, and P.J. Wray, eds., TMS-AIME, Warrendale, PA, 1982, p. 1.
4. A.J. DeArdo: *Can. Metall. Q.*, 1988, vol. 27, p. 141.
5. T. Gladman and F.B. Pickering: *J. Iron Steel Inst.*, 1967, June, p. 653.
6. R. Coladas, J. Masounave, G. Guerin, and J.-P. Bailon: *Met. Sci.*, 1977, vol. 11, p. 509.
7. G.R. Speich, L.J. Cuddy, C.R. Gordon, and A.J. DeArdo: in *Phase Transformations in Ferrous Alloys*, A.R. Marder and J.I. Goldstein, eds., TMS-AIME, Warrendale, PA, 1984, p. 341.
8. Y.C. Hirsch and B.A. Parker: *Met. Forum*, 1982, vol. 5, p. 41.
9. J.G. Speer, J.R. Michael, and S.S. Hansen: *Metall. Trans. A*, 1987, vol. 18A, pp. 211-22.
10. R.M. Smith and D.P. Dunne: *Mater. Forum*, 1988, vol. 11, p. 166.
11. M. Mohar Ali Bepari: *Metall. Trans. A*, 1989, vol. 20A, pp. 13-16.
12. A.J. DeArdo, J.M. Gray, and L. Meyer: in *Niobium*, H. Stuart, ed., TMS-AIME, Warrendale, PA, 1984, p. 685.
13. P.R. Rios: *Mater. Sci. Technol.*, 1988, vol. 4, p. 324.
14. E.K. Storms and N.H. Krikorian: *J. Phys. Chem.*, 1960, vol. 64, p. 1471.
15. K. Balasubramanian, A. Kroupa, and J.S. Kirkaldy: *Metall. Trans. A*, 1992, vol. 23A, pp. 729-44.
16. H. Nordberg and B. Aronsson: *J. Iron Steel Inst.*, 1968, Dec., p. 1263.
17. F. deKazinsky, A. Axnas, and P. Pachleiter: *Jernkontorets Ann.*, 1963, vol. 147, p. 408.
18. L. Meyer: *Z. Metallkd.*, 1967, vol. 58, p. 334.
19. R.P. Smith: *Trans. AIME*, 1966, vol. 236, p. 220.
20. K. Narita: *Trans. Iron Steel Inst. Jpn.*, 1975, vol. 15, p. 145.
21. T.H. Johansen, N. Christensen, and B. Augland: *Trans. AIME*, 1967, vol. 239, p. 1651.
22. T. Mori, M. Tokizane, K. Yamaguchi, E. Sunami and Y. Nakazima: *Tetsu-to-Hagané*, 1968, vol. 54, p. 763.
23. S. Koyama: *J. Jpn. Inst. Met.*, 1972, vol. 52, p. 1090.
24. R.C. Sharma, V.K. Lakshmanan, and J.S. Kirkaldy: *Metall. Trans. A*, 1984, vol. 15A, pp. 545-53.
25. V.K. Lakshmanan and J.S. Kirkaldy: *Metall. Trans. A*, 1984, vol. 15A, p. 541.
26. T. Nishizawa, H. Ohtani, and M. Hasebe: *CALPHAD*, 1985, vol. 9, p. 201.
27. H. Ohtani, M. Hasebe, and T. Nishizawa: *CALPHAD*, 1989, vol. 13, p. 183.
28. K. Balasubramanian and J.S. Kirkaldy: in *Advances in Phase Transitions*, J.D. Embury and G.R. Purdy, eds., Pergamon Press, Oxford, 1988, p. 37.
29. R.P. Smith: *Trans. AIME*, 1962, vol. 224, p. 190.
30. K.J. Irvine, F.B. Pickering, and T. Gladman: *J. Iron Steel Inst.*, 1967, Feb., p. 161.
31. T.M. Hoogendoorn and M.J. Spanraft: in *Microalloying 75*, M. Korchynsky, ed., Union Carbide Corporation, New York, NY, 1977, p. 75.
32. M.L. Santella: Ph.D. Thesis, University of Pittsburgh, Pittsburgh, PA, 1981.
33. R.C. Hudd, A. Jones, and M.N. Kale: *J. Iron Steel Inst.*, 1971, vol. 209, p. 121.
34. Y.D. Lee: *TMS Technical Paper No. F88-3*, TMS-AIME, Warrendale, PA, 1988, p. 1.
35. R.A. Swalin: *Thermodynamics of Solids*, 2nd ed., John Wiley and Sons, New York, NY, 1972, p. 165.
36. D.A. Porter and K.E. Easterling: *Phase Transformations in Metals and Alloys*, Van Nostrand Reinhold Co. LTD., Berkshire, United Kingdom, 1981, pp. 386-89.
37. T. Sakuma and R.W.K. Honeycombe: *Mater. Sci. Technol.*, 1985, vol. 1, p. 351.
38. R.F. Mehl: *Hardenability of Alloy Steels*, ASM, Cleveland, OH, 1939, p. 1.
39. C.I. Garcia, E.J. Palmiere, and A.J. DeArdo: *Mechanical Working and Steel Processing Proceedings*, The Iron and Steel Society, Warrendale, PA, 1989, p. 59.
40. G.F. Vander Voort: *Metallography: Principles and Practice*, McGraw-Hill Book Company, New York, NY, 1984, p. 538.
41. O. Kwon and A.J. DeArdo: *Acta Metall.*, 1991, vol. 39, p. 529.

42. T. Gladman: *Proc. R. Soc. London*, 1966, vol. 294, p. 298.
43. M. Hillert: *Acta Metall.*, 1965, vol. 13, p. 227.
44. S. Matsuda and N. Okumura: *Tetsu-to-Hagané*, 1976, vol. 62, p. 1209.
45. L.J. Cuddy: in *Thermomechanical Processing of Microalloyed Austenite*, A.J. DeArdo, G.A. Ratz, and P.J. Wray, eds., TMS-AIME, Warrendale, PA, 1982, p. 129.
46. L.J. Cuddy: *Metall. Trans. A*, 1981, vol. 12A, p. 1313.
47. L.J. Cuddy, J.J. Bauwin, and J.C. Raley: *Metall. Trans. A*, 1980, vol. 11A, pp. 381-86.
48. R.E. Smallman: *Modern Physical Metallurgy*, 4th ed., Butterworths, London, 1985, p. 380.
49. R.W. Cahn and P. Haasen: *Physical Metallurgy*, 3rd ed., Elsevier Science Publishers, Amsterdam, Holland, 1983, p. 934.
50. J. Chipman: *J. Iron Steel Inst.*, 1955, vol. 180, p. 97.
51. Y. Zheng, G. Fitzsimons, and A.J. DeArdo: in *HSLA Steels: Technology and Applications*, M. Korchynsky, ed., ASM INTERNATIONAL, Metals Park, OH, 1984, p. 85.
52. R.M. Fix, Y.Z. Zheng, and A.J. DeArdo: *Proc. Int. Conf. on HSLA Steels*, ASM INTERNATIONAL, Metals Park, OH, 1986, p. 219.